

# Slip-Jump Model for Carbon Combustion Synthesis of Complex Oxide Nanoparticles

A.A. Markov<sup>1</sup>, M.A. Hobosyan<sup>2</sup>, and K.S. Martirosyan<sup>2\*</sup>

<sup>1</sup>IPMech RAS, Moscow 119526, Russia

<sup>2</sup>Department of Physics, University of Texas at Rio Grande Valley, Brownsville, TX 78520, USA

## Article info

*Received:*  
2 February 2016

*Received and revised form:*  
20 March 2016

*Accepted:*  
26 April 2016

### Keywords:

slip-jump fluxes,  
transport intensification,  
carbon combustion,  
Ni-Zn ferrites, nanoparticles

## Abstract

Carbon Combustion Synthesis of Oxides (CCSO) is a promising method to produce submicron- and nano- sized complex oxides. The CCSO was successfully utilized for producing several complex oxides, a complete theoretical model including the sample porosity, flow parameters and reaction energetics is needed to predict the combustion parameters for CCSO. In this work, we studied the ignition temperature and combustion wave axial temperature distribution, activation energy, combustion heat and thermal losses for a typical CCSO synthesis for cylindrical samples of Ni-Zn ferrites with high (>85%) porosity. We developed a two level combustion model of chemically active nano-dispersed mixture, using the experimentally measured ignition temperature and combustion parameter values utilizing the slip-jump method for high Knudsen numbers. The theoretical predictions of highly porous samples when the flow resistivity is small and the gas can easily flow through the cylindrical sample are in good agreement with the experimental data. The calculation of combustion characteristics for the lower porosity values demonstrated that the surface combustion was dominated due to high gas flow resistivity of the sample. Finger combustion features were observed at this combustion mode.

## 1. Introduction

Recent experimental studies of convective and diffusion transfer in carbon nanotubes [1–3] showed acceleration of transfer on more than 2 orders of magnitude compared to the estimations based on theory of continuum media [4–7]. The intensification of transfer can be partially explained by direct modeling of motion of ensemble of molecules using the method of molecular dynamics. The length of mean free path of the gas molecules inside the pores of the carbon is exceeding the diameter of the pores. The reflection of the gas molecules from the nanotube boundaries dominates the rate of the reflection of gas molecules between each other and the Knudsen numbers may reach 10–70 values. However, the measured flows of the gas exceed the values estimated by the theory of Knudsen layers well over 10 to 100 times.

The experimental results mentioned above and the limitation of theoretical models stimulated the foundation of theory for the processes of thermal and mass transfer based on the effects of gas slip

and concentration and temperature jumps in the Knudsen layer [8]. The boundary conditions on the wall of the tubes taking into account the slip and jump of temperature for the large Knudsen numbers are given in the work by Cheng [9], where the focus of discussion is the case of a rarefied homogeneous gas flow without chemical reactions near the macro-scale objects. In addition it was confirmed the solutions for the stagnation region based on a single dissociation-recombination kinetic model show a substantial concentration jump across the shock, and extensive influence of surface cooling low Reynolds number [9]. The further development of the theory for supersonic flows of absolutely rarefied viscous gas around objects in the transitional regime of continuous to free molecular flow resulted to wide range of Knudsen number of incoming flow using both continuous and kinetic approaches [10]. A two-dimensional analysis with a first-order slip-velocity boundary condition in the Navier-Stokes equations displays that both compressibility and rarefied effects are present in long microchannels [11]. The continuous approach is

\* Corresponding author. E-mail: karen.martirosyan@utrgv.edu

based on the usage of specified conditions for the temperature jump on the surface of object.

In contrast to the macro-scaled combustion processes of carbon for the large Knudsen numbers presented in the work [8] gives the generalized approach of Cheng [9] for the combustion of nanoscale carbon particles. With the conditions of temperature jump of gas phase, also the boundary conditions of concentration jumps are introduced for the reacting gas components. The calculations of carbon combustion for the transitional regimes from the continuum to molecular flow regimes are performed, using the methods of molecular dynamics. The theory of slip and jump of temperature and concentration of gaseous mixture  $O_2$  and  $CO_2$  helped to understand the features of complex gas dynamics and thermal processes in the combustion wave for sub-micron scales, which is utilized in the synthesis of nano sized particles.

In this work we provide the theoretical and experimental study of the synthesis of Ni-Zn ferrite nanoparticles using the CCSO method [12–14]. Currently there is a lack of theory predicting combustion parameters for the synthesis of nanoparticles using CCSO. The combustion initiation temperature and the axial temperature distribution during the combustion, as well as the activation energy and reaction heat values were estimated experimentally. These values were used to develop a two level model of chemically active nano-dispersed mixture [15–19] which can be applied to the synthesis of nano-sized particles of  $Ni_{0.35}Zn_{0.65}Fe_2O_4$  based on kinetics [14] and processes of mass and thermal transfer in the isolated pore (meso-scale), which is a procedure of averaging the micro-scaled mass and thermal flows in the calculations of characteristic mixture in macro scale. The theoretical predictions and the experimental values of the combustion axial temperature distribution and combustion wave propagation characteristics are in good agreement for the highly porous (>85%) samples when the oxidizer can easily flow through the sample. In addition, the theoretical calculations for lower porosity values were performed, when the flow resistivity is high and surface combustion takes place, and the combustion parameters and regimes were predicted.

The defining equations in macro scale use the Euler formulations – the principles of mass, impulse and energy conservation for the leading phase, including the averaged micro-scaled flows, as well as equations for fractions of particles.

The effect of slip decelerates the combustion process when the slip parameters are small and the heating time is short. For this case, we observed a decrease of temperature (more than twice), signifi-

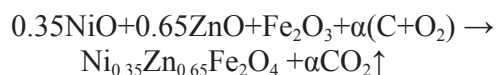
cant differences in the pressure distribution, and deceleration of carbon combustion. The intensive outflow of the gas from the combustion zone and from the sample in general results in the thermal losses and decelerates the combustion process during the slippage. The combustion transforms from the diffusion to the convective-diffusion regime.

In the case of intensive slip parameter, a non-monotonous dependence of temperature on the parameter of slippage values  $A_u$  is observed. In addition to the thermal outflow from the combustion zone in some cases increase of combustion efficiency during the slip increase was observed, due to the increased inflow of the oxidizer to the synthesis zone. In the case of intensive slip parameter values we have a non-monotonous dependence of temperature on the value of the  $A_u$ . In some cases, the thermal outflow from the combustion zone results in slowing down the synthesis and decrease in temperature while increasing the  $A_u$  parameter.

However, in other cases, in parallel to the thermal outflow from the combustion zone, we observed an effect of intensified combustion process, which was due to the increased inflow of the oxidizer to the combustion zone. This intensification of combustion results in increase of temperature, during which the sample is intensively heated through the extreme gas convection. Thus, the decrease of temperature while increasing the  $A_u$  parameter transforms into the increase of temperature due to the intensive heating of the whole sample during the extreme gas convection. An analogous effect of temperature increase takes place when the heating time of the sample and the oxygen supply rate is increased.

## 2. Experimental System and Procedure

The CCSO synthesis of the  $Ni_{0.35}Zn_{0.65}Fe_2O_4$  ferrite was via the reaction:



where  $2 < \alpha < 14$  [14]. Reagents were purchased from Sigma Aldrich and were used as received. The reagents included NiO (nano powder, < 50 nm),  $Fe_2O_3$  (nano powder, < 50 nm), ZnO (< 100 nm), and activated carbon (water content < 30 wt.%, 100 mesh).

The reagents were mixed in rotary ball mill in stainless steel jar with  $ZrO_2$  balls for 3 h (ball to mixture weight ratio was 6:1). The mixture was loosely filled in vertical quartz tube with 14 mm inner diameter, which had alumina foam to support the mixture and allow the oxygen flow (Fig. 1). The

height of the sample was 4 mm and the relative density  $\sim 0.12$ . The oxygen (99.994% purity, Air-gas) was fed by the flow rate 3 L/min, and the flow rate was measured both in the inlet and outlet of the reaction tube. The oxygen flow direction and the combustion wave direction were the same.

The combustion temperatures were measured with K type micro-thermocouples (Omega) placed inside the sample near the center and at the wall of the quartz tube. The thermocouples signals were recorded with the rate of 1 kHz and processed by an Omega data acquisition board connected to a PC. The combustion wave was initiated with a short ( $\sim 1$  s) laser pulse (1.5 W) and the combustion process was recorded by high-speed camera (1000 Hz) to estimate combustion front motion behavior and velocity. The thermo-gravimetric (TG) and differential thermal analysis (DTA) was performed by using Differential Scanning Calorimeter (DSC) with the sensitivity of  $0.1 \mu\text{g}$  (Q-600, TA Instruments). The measurements were made in oxygen atmosphere (99.994% purity).

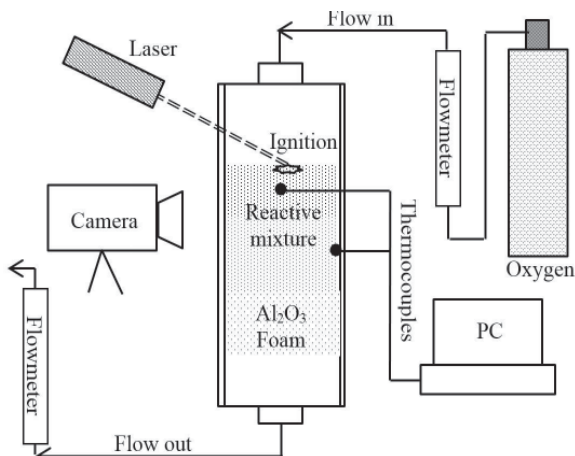


Fig. 1. Schematics of the experimental setup.

### 3. Experimental results

Figure 2a is representing the TG/DTA results for the carbon at heating rate  $20 \text{ }^\circ\text{C}/\text{min}$ . The blue line represents the weight change, the green line is the heat flow, and the red line indicates the points through which the heat flow peaks are integrated for the thermal effects. The evaporation of absorbed water completes at around  $100 \text{ }^\circ\text{C}$  with the energy consumption of about  $822 \text{ J/g}$ , when the mass change due to evaporation was  $23.64 \text{ wt.}\%$ . This graph clearly shows that the ignition of carbon combustion starts at  $\sim 405 \text{ }^\circ\text{C}$  and the combustion releases  $7645 \text{ J/g}$  energy. Figure 2b is representing the same results for the system, where  $\alpha = 10$ . Due to smaller fraction of carbon, the absorbed water is about  $9 \text{ wt.}\%$  of the overall mixture with evaporation energy  $\sim 208 \text{ J/g}$  before  $100 \text{ }^\circ\text{C}$ . The ignition temperature was  $366 \text{ }^\circ\text{C}$  and the combustion energy estimated  $5470 \text{ J/g}$ . Thus, the formation of oxides is endothermic process that consumes  $\sim 2175 \text{ J/g}$  energy.

We estimated the activation energy from the DTA data by using the isoconversional method suggested by Starink [20], which was shown to provide a more accurate value than the Kissinger and Ozawa methods. The Starink method determines the activation energy from the equation:

$$\ln\left\{\frac{\beta}{T^{1.92}}\right\} = -1.0008 \frac{E_a}{RT} + \text{const},$$

where  $E_a$  is the apparent activation energy (in  $\text{kJ/mol}$ ),  $\beta$  is the heating rate in thermal analysis (in  $\text{K/min}$ ),  $T$  is the peak temperature of the exothermic curve (in  $\text{K}$ ), and  $R$  the universal gas constant.  $E_a$  is estimated from the slope of the graph of  $\ln(\beta/T^{1.92})$  vs.  $1/T$ .

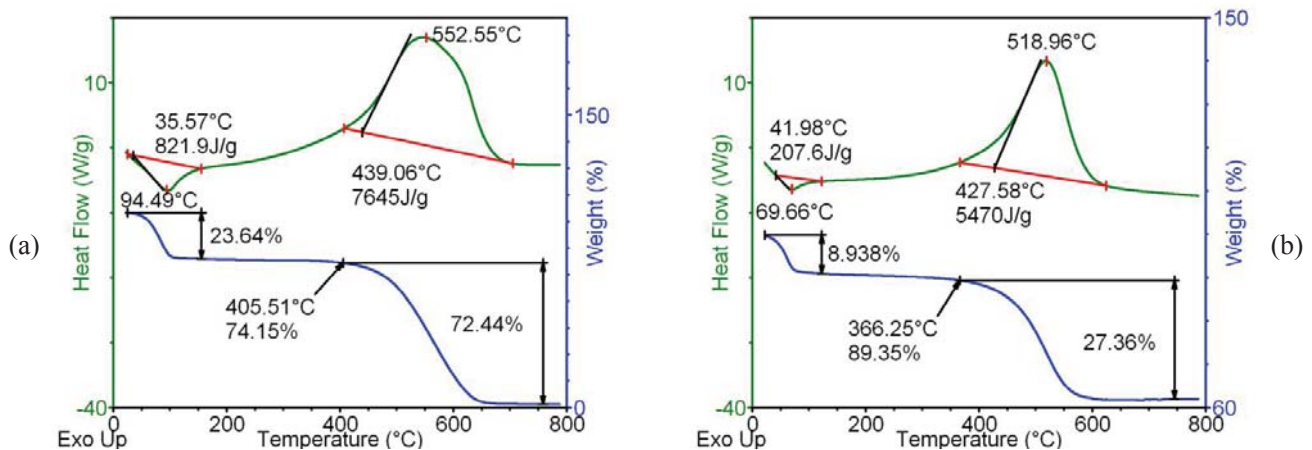


Fig. 2. a) DTA-TG curves for the carbon combustion at  $20 \text{ }^\circ\text{C}/\text{min}$  heating rate, b) DTA-TG curves for the mixture with  $\alpha = 10$  at  $20 \text{ }^\circ\text{C}/\text{min}$  heating rate.

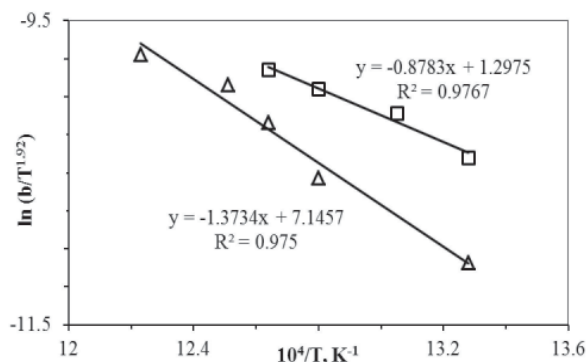
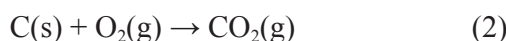


Fig. 3. Arrhenius plots for the carbon combustion (triangles) and combustion of  $\alpha = 10$  mixture (squares) at heating rates 5–25 °C/min.

We estimated the activation energy for the carbon combustion from the slope of the graph shown in Fig. 3 as  $114 \pm 3.4$  kJ/mol, while the activation energy for the carbon combustion of nickel–zinc ferrite at  $\alpha = 10$  was  $73 \pm 2.2$  kJ/mol. These estimates together with the ignition temperatures and combustion energy values for each system, as well as the combustion wave temperature axial distribution measurements were used to perform theoretical calculations and compare the results with the experimental measurements. The data used in the theoretical calculations are presented in Table 1.

#### 4. Mathematical model

The CCSO synthesis of the  $\text{Ni}_{0.35}\text{Zn}_{0.65}\text{Fe}_2\text{O}_4$  ferrite proceeds according to the reaction above. Let us consider the kinetics of combustion in a tube under excess amount of oxygen:



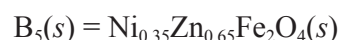
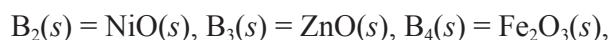
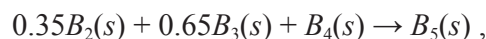
where (g) denotes gas and (s) denotes solid phase. The molar masses of reagents  $\text{A}_1(\text{g})$ ,  $\text{B}(\text{s})$  and the product  $\text{A}_2(\text{g})$ , and their thermal capacities satisfy the relations:

$$\frac{M_{1g}}{M_{1s}} + 1 = \frac{M_{2g}}{M_{1s}} \quad \frac{M_{1g}}{M_{1s}} C_{1g} + C_{1s} = \frac{M_{2g}}{M_{1s}} C_{2g} \quad (3)$$

where  $M$  denotes the molar mass, and  $c$  denotes the thermal capacity of the corresponding component. We will use the effective density values denoted by  $\bar{\rho}$ :

$$\bar{\rho}_g = \bar{\rho}_{1g} + \bar{\rho}_{2g} \quad (4)$$

The simulation of zinc nickel ferrite synthesis is based on following kinetics:



The molar masses of reagents, products and their thermal capacities satisfy the following relations:

$$\frac{0.35M_{2s}}{M_{4s}} + \frac{0.65M_{3s}}{M_{4s}} + 1 = 0, c_{4s} = -\left(c_{2s} \frac{0.35M_{2s}}{M_{4s}} + \frac{0.65M_{3s}}{M_{4s}}\right)$$

We apply the time and length scales for combustion proposed by Frank-Kamenetskii [21].

The characteristic time scale  $t_0$  and length scale  $l_0$  are as follows

$$t_0 = \frac{\exp\left(\frac{E}{RT_0}\right)}{k} \quad l_0 = \sqrt{\frac{\lambda_0 t_0}{c_v \rho_0}} \quad (5)$$

$\lambda_0$  is the referred thermal conductivity,  $R$  is the universal gas constant. Below we will use the transformed non-dimensional variables marked tilde above the letters. For Cartesian coordinates the variables follow:

$$\tilde{x}_k = x_k / l_0, \tilde{t}_k = t / t_0, \tilde{u}_k = u_k / u_0, k = 1, 2, 3; u_0 = l_0 / t_0 \quad (6)$$

$$\tilde{p} = p / p_0, \tilde{\rho}_g = \bar{\rho}_g / \rho_0, \tilde{\rho}_{jg} = \rho_{jg} / \rho_0, j = 1, 2; \tilde{\rho}_s = \bar{\rho}_s / \rho_0 \quad (7)$$

**Table 1**

Experimental data used in theoretical calculations

System	$T_{\text{ign}}, ^\circ\text{C}$	$E_{\text{act}}, \text{kJ/mol}$	$E_{\text{heat}}, \text{kJ/g}$	Porosity, vol. %	$T_{\text{c,max}}, ^\circ\text{C}$	$T_{\text{wall}}, ^\circ\text{C}$	Normalize $\text{O}_2$ flow rate, $\text{Lmin}^{-1}\text{cm}^{-2}$
Carbon combustion in oxygen	405	$114 \pm 3.4$	7645	88	1108	570	1.95
Mixture with $\alpha = 10$ in oxygen	336	$73 \pm 2.2$	5770	88	780	520	1.95

Here, the characteristic pressure is

$$p_0 = \frac{R\rho_0 T_0}{M_0} \quad (8)$$

where  $T_0 = 1273$  K is the characteristic temperature. The main similarity parameters will be

$$\beta = \frac{RT_0}{E}, \quad \text{and} \quad \gamma = \frac{c_p T_0 \beta}{Q} \quad (9)$$

Where  $Q$  is the combustion heat and  $E$  is the activation energy. The non-dimensional temperature is expressed as

$$\tilde{T} = \frac{(T - T_0)E}{RT_0^2}, \quad \frac{T}{T_0} = 1 + \beta\tilde{T} \quad (10)$$

The non-dimensional variables are applied for numerical simulation.

For non-dimensional variables

$$\frac{\rho_0 c_v}{t_0} = \frac{\lambda_0}{l_0^2}, \quad T = T_0(1 + \beta\tilde{T}) \quad (11)$$

The solid-gas concentration flux jump equation reads: the mass fluxes caused by chemical reaction are as follows:

$$J_{s \rightarrow g}^{macro} = \rho_{1s} \rho_{1g} k \exp\left(\frac{T_g}{\beta T_g + 1}\right), \quad J_{l \rightarrow g}^{macro} = \frac{M_{lg}}{M_{1s}} J_{s \rightarrow g}^{macro}, \quad l = 1, 2 \quad (12)$$

$$J_{s \rightarrow g}^{macro} = \rho_{1s} \rho_{1g} k \exp\left(\frac{T_g}{\beta T_g + 1}\right), \quad J_{l \rightarrow g}^{macro} = \frac{M_{lg}}{M_s} J_{s \rightarrow g}^{macro}, \quad l = 1, 2$$

Here,

$$\rho_{1s} = (1 - \chi)\bar{\rho}_{1s}, \quad \rho_{1g} = \chi\bar{\rho}_{1g}, \quad \rho_{2g} = \chi\bar{\rho}_{2g}$$

where  $\chi$  is the porosity. Mass fractions  $C_1$  and  $C_2$  are as follows

$$\bar{\rho}_{1g} = \bar{\rho}_g C_1, \quad C_2 = 1 - C_1 \quad (13)$$

The equation of state reads as

$$P_g = \bar{\rho}_g T_g \frac{R}{M_0} \quad (14)$$

Let us note that we consider the pore surface values  $\bar{\rho}_{gsf,1}, \bar{\rho}_{gsf,2}$ , of gas components along with the values  $\bar{\rho}_{1g}, \bar{\rho}_{2g}$  of these components in side the pores. Note that the surface is denoted with capital ‘‘S’’ while the solid phase components are denoted with lower case ‘‘s’’. The basic equations for carbon combustion at macro level in non-dimensional variables are presented by using the flux jump values and the equation of mass, energy and momentum conservation as follow (tilde denoting non dimensional value hereafter is omitted for brevity):

$$\frac{\partial \chi \rho_g}{\partial t} + \nabla \cdot (\chi \rho_g u) = (1 - \chi) (J_{s \rightarrow g}^{macro} + J_{C,jump,1}^{macro} + J_{C,jump,2}^{macro}) \quad (15)$$

$$J_{C,jump,l}^{macro} = D_T A_T Pe_l \sqrt{\rho_g p_g} \beta (-T_g + T_s) \left( \frac{1 + \beta T_g}{1 + \beta T_s} \right)^\alpha + A_{C,l} Pe_l (-\rho_g B_l + \rho_{gsf,l}) \quad (16)$$

Here,  $D_T$  is the thermal diffusivity coefficient,  $Pe_l$  are the Peclet numbers  $Pe_l = \frac{u_0 l_0}{D_{l,0}}$ ,  $l = 1, 2$ ,  $u_0$  is the referred velocity  $u_0 = \frac{l_0}{t_0}$ .  $A_T$  and  $A_{C,l}$  are temperature and concentration jump parameters  $A_T = \frac{2\chi b_T l_0^2 \sqrt{\rho_0 P_0}}{r^1 \mu_0}$  and  $A_{C,l} = B_{C,l} \frac{2\chi t_0}{r_1} b_l$ , where  $b_T$  is the slip parameter:

$$b_T = \frac{2 - \alpha}{\alpha} \sqrt{\frac{\pi}{2}} \frac{2\gamma}{\gamma + 1}, \quad \alpha \text{ is the thermal accommodation coefficient, } b_l \text{ denotes the wall constant for the specie jump that is similar to the value of } b_u \text{ for the velocity slip: } b_u = \frac{\theta}{2 - \theta} \sqrt{\frac{2}{\pi}}, \text{ where } \theta \text{ is the reflection coefficient.}$$

For pores of submicron size  $r_1 \approx 5 \cdot 10^{-7}$  m, using

$$\sqrt{\rho_0 P_0} \approx \sqrt{10^{-3} \cdot 10^5} = 10, \quad l_0 \approx 10^{-5}, \quad T_0 \approx 10^3, \quad \mu_g = 5 \cdot 10^{-5}$$

we estimated  $A_u \approx 200\chi b_u$ ,  $A_{C,l} \approx 10^3\chi b_l$ , and  $A_T \approx 200\chi b_T$

For nanoscale pores  $r_1 \approx 5 \cdot 10^{-8}$  m the intensities of velocity slip and concentration and temperature jump increase to one order of magnitude. The relative concentration of oxygen and carbon dioxide

$$\frac{\partial \chi \rho_g C_1}{\partial t} + \nabla \cdot (\chi \rho_g C_1 u) = \nabla \cdot \left( \frac{D_{1g}}{pe_1} \rho_g \nabla C_1 \right) - \frac{M_{1g}}{M_{1s}} J_{s \rightarrow g}^{macro} + J_{C,jump,1}^{macro}, \quad C_2 = 1 - C_1 \quad (17)$$

We note that

$$\rho_{1g} = \rho_{O_2(g)}, \rho_{2g} = \rho_{CO_2(g)}, \rho_s = \rho_{C(s)}, \text{ and } c_1 = \frac{\rho_{1g}}{\rho_g}$$

$$J_{C,jump,l}^{macro} = A_{C,l} \left( -\rho_g C_{g,l} + \rho_{gSf,l} \right) + D_T Pe_l Q_{jump}^{macro}, l=1,2$$

The equation for gas concentrations at the pore surface

$$\frac{\partial \rho_{gSf,l}}{\partial t} = -J_{gSf,l}^{macro}, J_{gSf,l} = \rho_s \rho_{gSf,l} k \exp\left(\frac{T_s}{\beta T_s + 1}\right) \quad (18)$$

$$\frac{\partial \rho_{gSf,l}}{\partial t} = -J_{gSf,l}^{macro}, J_{gSf,l}^{macro} = \frac{M_{1g}}{M_{1S}} J_{gSf,l}, l=1,2, \quad (19)$$

where  $\rho_{gSf,1}, \rho_{gSf,2}$  are the values of gas densities  $\rho_{1g}, \rho_{2g}$  at the surface of pores and  $T_s$  is the solid carbon temperature. The carbon concentration denotes:

$$\frac{\partial \rho_s}{\partial t} = -J_{s \rightarrow g}^{macro} \quad (20)$$

The equations for ferrite synthesis reads:

$$\begin{aligned} \frac{\partial \rho_{2s}}{\partial t} &= -0.35 \frac{M_{2S}}{M_{4S}} J_s, \quad \frac{\partial \rho_{3s}}{\partial t} = -0.65 \frac{M_{3S}}{M_{4S}} J_s, \\ \frac{\partial \rho_{4s}}{\partial t} &= -J_s, \quad \frac{\partial \rho_{5s}}{\partial t} = \frac{M_{5S}}{M_{4S}} J_s, \end{aligned}$$

where

$$J_s = (1 - \chi) k_2 (\rho_{2s})^{0.35} (\rho_{3s})^{0.65} (\rho_{4s}) \exp\left(\frac{T_s}{\beta T_s + 1}\right)$$

The equation of gas mixture velocity:

$$\begin{aligned} \frac{\partial \chi \rho_g u}{\partial t} + \nabla \cdot (\chi \rho_g u u) &= S_V + J_{slip}^{macro} - Ma^{-2} \nabla P_g + Re^{-1} \nabla \cdot \tau; \\ \tau &= \mu \left[ \nabla u + (\nabla u)^T - \frac{2}{3} (\nabla \cdot u) I \right] \end{aligned} \quad (21)$$

Where the distributed pore resistivity is

$$(S_V)_i = -u_i k_i, k_i = a_i |u| + \zeta_i, i = 1,2,3; \quad (22)$$

$\alpha_i$  and  $\zeta_i$  are respectively for non-linear and linear coefficient parts of the distributed pore resistivity.  $Ma$  is the Mach number;  $Re$  is the Reynolds number

$Re_0 = \frac{u_0 l_0 \rho_0}{\mu_0}$  and the slip flux

$$J_{slip}^{macro} = A_u u \sqrt{p_g \rho_g} \quad (23)$$

The heat balance for gas

$$\chi \bar{\rho}_g C_g \left( \frac{\partial T_g}{\partial t} + u \cdot \nabla T_g \right) = \nabla \cdot (\lambda_g \nabla T_g) + Q_g^{macro} + Q_{jump}^{macro}, Q_g^{macro} = Q_{s \rightarrow g}^{macro} \quad (24)$$

The heat balance for solid

$$\rho_s c_s \frac{\partial T_s}{\partial t} = \nabla \cdot (\lambda_s \nabla T_s) + Q_{gs}^{macro}, Q_{gs}^{macro} = Q_{gs} \quad (25)$$

The temperature-jump flux will be corresponding to be

$$Q_{jump}^{macro} = A_T \sqrt{\rho_g p_g} \left( (-T_g + T_s) + \frac{b_w}{b_{T\beta}} (1 + \beta T_s) \right) \left( \frac{1 + \beta T_g}{1 + \beta T_s} \right)^\alpha \quad (26)$$

where  $0 \leq b_w \leq 1$ .

## 5. Computational results and discussion

We present the numerical modeling of  $Ni_{0.35}Zn_{0.65}Fe_2O_4$  synthesis at both high and low porosity values. In the calculation, we observed two distinct modes of synthesis: axial combustion and surface combustion. We studied the characteristics of these synthesis modes for nanoparticle size range between 10–100 nm. The model is presented for the synthesis taking into account the gas slip, concentration and temperature jumps for  $O_2$  and  $CO_2$  at the surface of pores. We observed some cases of finger combustion for instable temperature fields. We compare the features of synthesis of coarser particles of ~10 micron with the synthesis of nanoparticles of ~100 nm at the porosity value 0.05%. The synthesis of coarser particles takes place faster, because during the synthesis of coarser particles, there is no gas slippage on the surface of pores, and as a result, there is no thermal loss from the zone of combustion.

Figure 4 demonstrates the comparison modeling with experiment, when no reagents of ferrite synthesis were considered. The temperature of gas at the axis of symmetry and at the outer boundary of the sample is shown in Fig. 4a and 4b, respectively. The slip jump intensities are as follows  $A_u = 100$ ,  $A_T = A_{O_2} = A_{CO_2} = 10$ . The satisfactory agreement can be seen in the Fig. 4c that presents the comparison of simulation of nickel zinc ferrite synthesis via carbon combustion with the experimental data. The discrepancy of data is less than 15%. The heat loss during the ferrite synthesis was evaluated using the experimental investigation. We estimated the thermal parameter of synthesis as follows  $Q_2 = -0.01$ .

The slip and jump intensities were  $A_u = 100$ ,  $A_T = A_{O_2} + A_{CO_2} + 10$ .

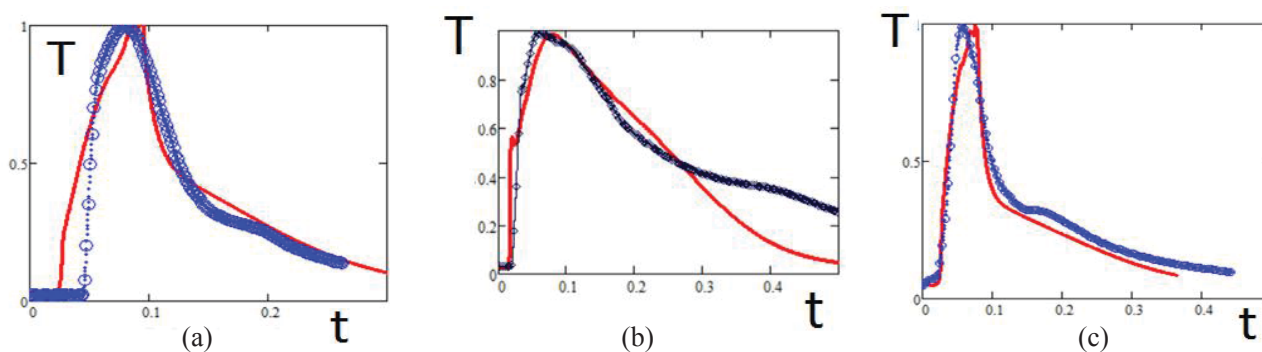


Fig. 4. Solid and dots lines refer to computation and experimental values, respectively for pure carbon combustion; i.e. when no reagents were considered: (a) – The time history of gas temperature at the axis of symmetry ( $r = 0, x$ ) for position (0, 0, 3); (b) – The time history of gas temperature at the outer boundary ( $r = 1, x$ ) of the sample for position (1, 0, 3). (c) – The time history of gas temperature at the axis of symmetry ( $r = 0, x$ ) for position, solid and dots lines refer to computation and experimental values, respectively for nickel zinc ferrite synthesis via carbon combustion.

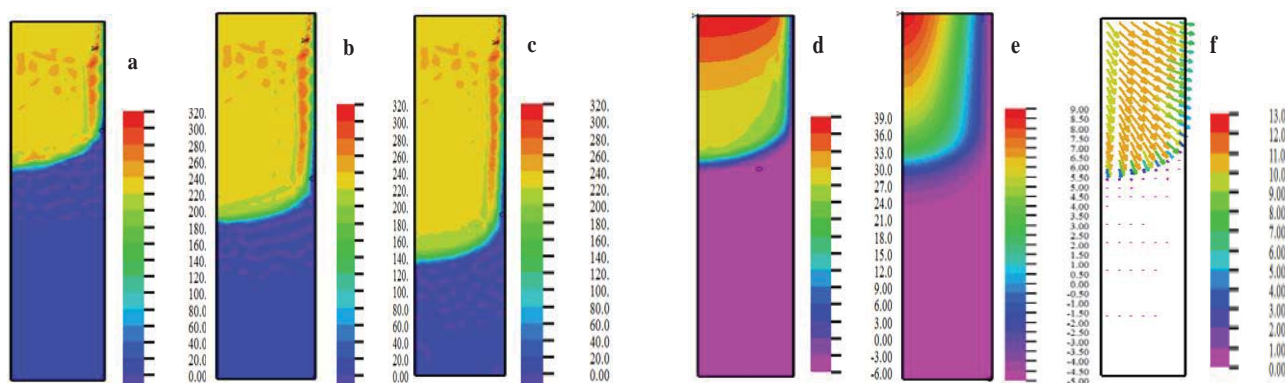


Fig. 5. Nickel zinc ferrite  $\text{Fe}_r(t, x, r)$  distributions at (a) –  $t = 0.2$ ; (b) –  $t = 0.3$ , (c) –  $t = 0.4$ . The temperature of gas (d) –  $T_g(0.2, x, r)$ ; solid (e) –  $T_s(0.2, x, r)$  and velocity of gas (f) –  $u(0.2, x, r)$  distributions at  $t = 0.2$  with porosity of 40%.

The simulation of nickel zinc ferrite synthesis for fast and slow heat exchange between gas and solid in the sample of large porosity 40% is shown in Figs. 5 and 6. The ferrite concentrations at subsequent moments of time are presented in Fig. 5, which illustrates the actual rate of ferrite synthesis and the non-uniformity of ferrite distribution. The synthesis of ferrite nanoparticles was modeled via axial carbon combustion  $J_T = \text{const}$ ,  $Q_2 = -0.01$ . Firstly, the modeling of fast thermal exchange between gaseous and solid phases during synthesis is considered. The distribution of gas and solid temperature and gas velocity at time  $t = 0.2$  is shown in Fig. 6 a-c. In spite of rather fast heat exchange between gas and solid, the temperature of solid phase is four times less than the temperature of gas. According to these results fast heat transfer occurs between gas and solid, when the heat transfer coefficient is  $\kappa = 1500$ . The slippage takes place at the pore surface only, i.e. no slippage at the outer wall is considered. The slip and jump intensities are as follows  $A_u = 100$ ,  $A_T = A_{O_2} = A_{CO_2} = 10$ . The interfacial interactions among the surface and gas molecules lead to inelastic reflections, due to the long-range interaction forces between the gas and surface molecules.

In Fig. 6 the slow heat transfer between gas and solid is shown, when the heat transfer coefficient is  $\kappa = 1$ . The slip and jump parameters are the same as in Fig. 5. The nickel zinc ferrite synthesis was simulated taking into account the activation energy and heat loss values obtained during our experimental study. The temperature of gas and solid differs more significantly for slow heat transfer between gas and solid. We can see the formation of local high temperature zones presented in Fig. 6 (a) caused by combustion instability due to outer boundary heat loss. These local regions of high gas temperature can be explained by a finger-like instability of combustion [15, 16]. The finger-like structure of temperature was observed experimentally [12] during the CCSO for ferrite synthesis. The non-uniformity of gas temperature causes a non-uniformity of ferrite density distribution and the process of synthesis as well as shown in the Fig. 7. The rate of ferrite synthesis for slow heat transfer between gas and solid can be seen. Let us note that fingers mode are not found at  $t = 0.1$  (see Fig. 8 (c)), however are structured later at  $t = 0.2$ . The comparison of Fig. 5 (a) and Fig. 6 (c) allows us to conclude that slower heat transfer between gas and solid lead to faster synthesis of nanoparticles.

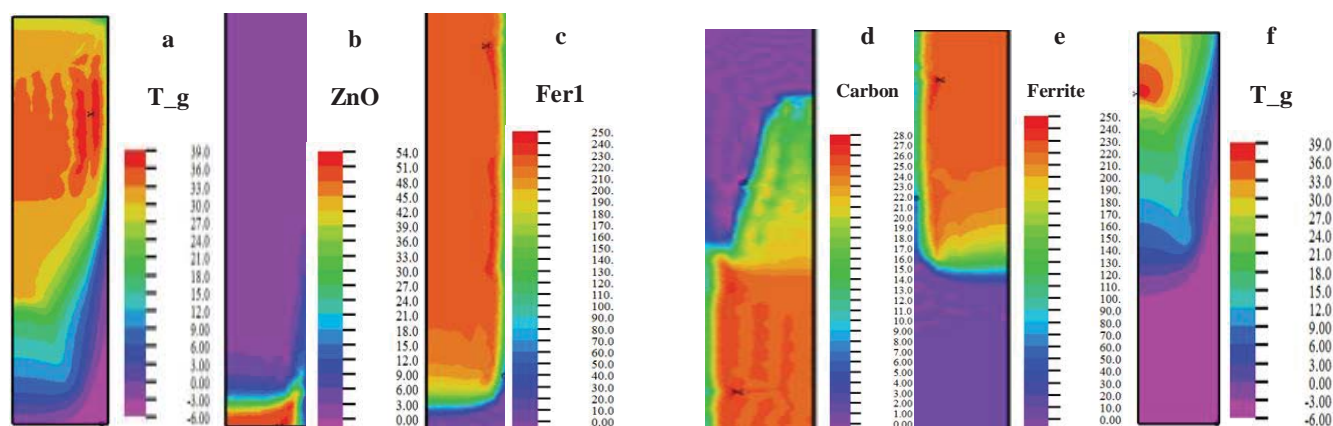


Fig. 6. (a) – Gas temperature  $T_g$  (0.2,  $x$ ,  $r$ ); (b) – zinc oxide ZnO (0.2,  $x$ ,  $r$ ); (c) – nickel zinc ferrite concentration Fer1 (0.2,  $x$ ,  $r$ ) at  $t = 0.2$ . (d) – Carbon C (0.1,  $x$ ,  $r$ ); (e) – nickel zinc ferrite Fer (0.1,  $x$ ,  $r$ ); (f) – concentration and gas temperature distribution  $T_g$  (0.1,  $x$ ,  $r$ ) at time  $t = 0.1$  is presented when  $A_T = A_{O_2} = A_{CO_2} = 10$  and porosity is 40%. Slip intensity effect is  $A_u = 100$ .

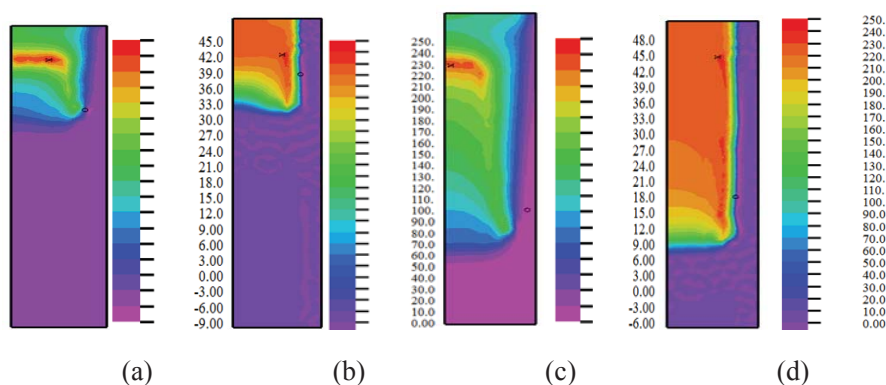


Fig. 7. Surface combustion: gas temperature  $T_g$  (0.02,  $x$ ,  $r$ ) (a) and nickel zinc ferrite concentration Fer1 (0.02,  $x$ ,  $r$ ) (b) at  $t = 0.02$ ; and gas temperature  $T_g$  (0.04,  $x$ ,  $r$ ) (c) and nickel zinc ferrite concentration Fer1 (0.04,  $x$ ,  $r$ ) (d) at time  $t = 0.04$ . The calculations are presented when  $A_T = A_{O_2} = A_{CO_2} = 10$  and porosity is 0.05%. Slip intensity effect is  $A_u = 100$ .

In Fig. 8 the nickel zinc ferrite synthesis is presented for small porosity of 0.05%, when large resistance for oxygen flux takes place and surface combustion occurs. The slip and jump intensities are the same as in previous case. The large particles (with several microns in diameter) of nickel zinc ferrite synthesis were simulated neglecting the slip and jump effects, since the Knudsen number was sufficiently small. These results demonstrate that the synthesis of large particles runs faster compared to the nanoscale particles, because the slippage results in heat loss from the combustion domain.

The performed systematical study of the slip and jump behavior reveals the effects of Knudsen layers on the thermal and mass transfers in the large interval of jump and slip parameters. The intensities of temperature and gas component concentration jumps are determined by the thermal diffusion as well as by the thermal coefficient of accommoda-

tion of molecules. The value of slippage depends on the coefficient of reflection of molecules from the wall of the tube and the pores. There is slowing down of the synthesis when the parameter of slippage grows from  $A_u = 1$  to  $A_u = 10$ .

## 6. Conclusions

For the modeling of nickel zinc ferrite synthesis, the macro fluxes caused by the gas slip, temperature and concentration jumps at the submicron pore surface are crucial. The synthesis can be simulated via the carbon combustion in a sample using the mechanics of continuum media supplemented with the effect of Knudsen layer. Thus, the effect of slippage slows down the combustion process. The lowering of temperature causes significant difference in the pressure distribution. The intensive outflow of the gas from the combustion zone and from the

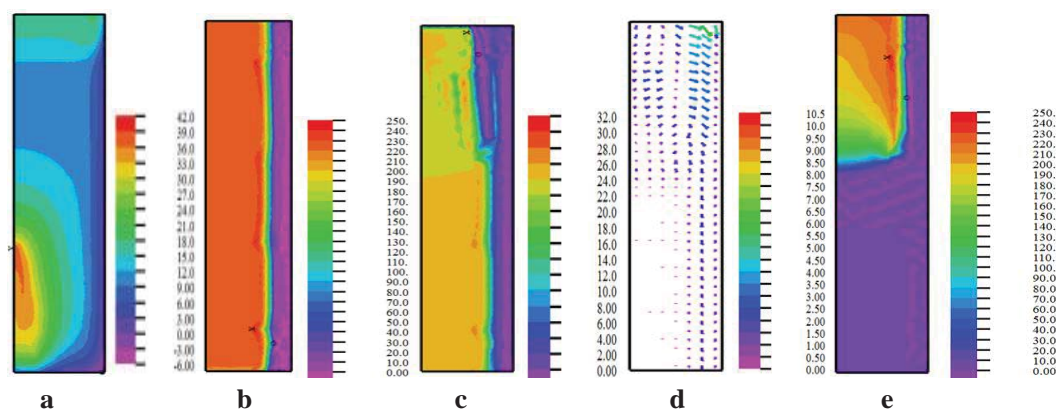


Fig. 8. Surface combustion: (a) – gas temperature  $T_g$  (0.1,  $x$ ,  $r$ ); (b) – nickel zinc ferrite concentration  $Fer1$  (0.1,  $x$ ,  $r$ ) at  $t = 0.1$ ; (c) – the carbon concentration  $C$  (0.02,  $x$ ,  $r$ ); (d) – gas velocity (0.02,  $x$ ,  $r$ ); (e) – nickel zinc ferrite concentration  $Fer1$  (0.02,  $x$ ,  $r$ ) at  $t = 0.02$ . For all these cases the parameters  $A_T = A_{O_2} = A_{CO_2} = 0$ , porosity of 0.05% and slip intensity effect is  $A_u = 0$ .

sample in general results in the thermal losses and slows down the combustion in case of slippage. The combustion transforms from the diffusion regime to convective-diffusion regime. At the high slippage parameter value there is non-monotonic dependence of temperature on the value of  $A_u$ . The stage of temperature decreasing while the parameter increases, transforms to increasing of temperature due to intensive heating of the whole sample at the extreme gas convection. The simulation result shows good agreement with the experimental investigation of nickel zinc ferrite synthesis.

## Acknowledgements

The financial support of this research by the Russian Foundation for Basic Research grant no. 14-08-00664 is gratefully acknowledged.

## References

- [1]. M. Kurzyp, C.A. Mills, R. Rhodes, T.R. Pozegic, C.T.G. Smith, M.J. Beliatas, L.J. Rozanski, A. Werbowy, and S.R.P. Silva, *J. Phys. D: Appl. Phys.* 48 (11) (2015) 115305.
- [2]. Jan Eijkel, *Lab Chip* 7 (2007) 299–301.
- [3]. Gerhard Hummer, Jayendran C. Rasiaiah, and Jerzy P. Noworyta. *Nature* 414 (6860) (2001) 188–190.
- [4]. A. Kalra, Sh. Garde, and G. Hummer, *Proceedings of the National Academy of Sciences* 100 (18) (2003) 10175–10180.
- [5]. Neto, Chiara, Drew R. Evans, Elmar Bonaccorso, Hans-Jürgen Butt, and Vincent SJ Craig. *Rep. Prog. Phys.* 68 (12) (2005) 2859–2897.
- [6]. Ajdari, Armand, and Lydéric Bocquet. *Phys. Rev. Lett.* 96 (18) (2006) 186102.
- [7]. Holt, Jason K., Hyung Gyu Park, Yinmin Wang, Michael Stadermann, Alexander B. Artyukhin, Costas P. Grigoropoulos, Aleksandr Noy, and Olgica Bakajin, *Science* 312 (5776) (2006) 1034–1037.
- [8]. A.A. Markov, *Computers & Fluids* 99 (2014) 83–92.
- [9]. Cheng, Hsien K. The blunt-body problem in hypersonic flow at low Reynolds number. No. AF1285A10. CORNELL AERONAUTICAL LAB INC BUFFALO NY, 1963.
- [10]. I.G. Brykina, B.V. Rogov and G.A. Tirskiy, *J. Appl. Math. Mech.* 73 (5) (2009) 502–513.
- [11]. Errol B. Arkilic, Martin A. Schmidt, and Kenneth S. Breuer, *Journal of Microelectromechanical Systems* 6 (2) (1997) 167–178.
- [12]. Karen S. Martirosyan, and Dan Luss. “Carbon combustion synthesis of oxides.” U.S. Patent 7,897,135, issued March 1, 2011.
- [13]. K. S. Martirosyan, and D. Luss, *AIChE J.* 51 (10) (2005) 2801–2810.
- [14]. K.S. Martirosyan, and D. Luss, *Ind. & Eng. Chem. Res.* 46 (5) (2007) 1492–1499.
- [15]. Andrey A. Markov, *Computers & Fluids* 38 (7) (2009) 1435–1444.
- [16]. Andrey A. Markov, Igor A. Filimonov, and Karen S. Martirosyan, *Journal of Computational Physics* 231 (20) (2012) 6714–6724.
- [17]. A.A. Markov, I.A. Filimonov, and K.S. Martirosyan, *Int. J. Self-Propag. High-Temp Synth.* 22 (1) (2013) 11–17.
- [18]. A. Markov, *Computational Fluid Dynamics Review* 368 (2010) 583–600.
- [19]. Andrey Markov, Igor Filimonov, and Karen Martirosyan. “Thermal reaction wave simulation using micro and macro scale interaction model.” In *Computational Fluid Dynamics 2010*, pp. 929–936. Springer Berlin Heidelberg, 2011.
- [20]. M.J. Starink. *Thermochim. Acta* 404 (1) (2003) 163–176.
- [21]. D.A. Frank-Kamenetskii, *Diffusion and Heat Exchange in Chemical Kinetics*, Princeton Legacy Library, p. 384, 2015.

## List of notations

$T_0 = 1273 \text{ K}$	Referred temperature
$T'$	Dimensional temperature
$T = \frac{T'}{T_0}$	Dimensionless temperature
$\tilde{T} = \frac{T-1}{\beta}$	Dimensionless normalized temperature
$T_g T_s$	Gas temperature and solid phase temperature
$T_{\text{ignit}}$	Ignition temperature
$T_{\text{initial}} = -\frac{1}{\gamma}$	Initial temperature of the sample
$C_{pk}$	Specific capacity at constant pressure for $k$ -specie
$n_p$	Numerical density of solid particles
$\rho_{lg}, l = 2$	Densities of gas species
$\rho_g = \rho_{1g} + \rho_{2g}$	Density of gas mixture
$\bar{\rho}_g, \bar{\rho}_s$ $\rho_g = \chi \bar{\rho}_g$ $\rho_s = (1-\chi)\bar{\rho}_s, \bar{\rho}_s = \bar{\rho}_s = \bar{\rho}_{c(s)}$	Effective values of gas density $\rho_g$ and solid density $\rho_s$
$\bar{\rho}_{1g} = \bar{\rho}_{O_2(g)}, \bar{\rho}_{2g} = \bar{\rho}_{CO_2(g)}$	Effective density of gas species
$\bar{\rho}_{lgSf}$	The values of gas densities $\bar{\rho}_{lg}, l=1,2$ at the pore surface
$\beta = \frac{RT_0}{E}$	Dimensionless parameter
$\gamma = \frac{c_p T_0 \beta}{Q}$	Dimensionless parameter (Zeldovich number)
$Pe_l = \frac{u_0 l_0}{D_{l,0}}, l = 1,2$	Peclet numbers
$u_0 = \frac{l_0}{t_0}$	Referred velocity
$Re_0 = \frac{u_0 l_0 \rho_0}{\mu_0}$	Reynolds number
$(S_v)_i = -u_i \kappa_i, k_i = \alpha_i  u  + \zeta_i, i = 1,2,3$	Porous resistance coefficient

$J_{\text{slip}}^{\text{macro}} = A_u u \sqrt{p\rho}$	Macro momentum flux due to velocity slip at the boundaries of pores
$J_{C,jump,l}^{\text{macro}}$	Macro mass flux of specie component due to its concentration jump at the pores boundary
$\chi$	Porosity coefficient
$M_j$	Molar mass of specie
$P_0 = \frac{R\rho_0 T_0}{M_0}$	Referred pressure
$\mu_0$	Referred gas viscosity
$\lambda_0$	Referred thermal conductivity
$Ma_0$	Mach number
$V(x, y, z)$	Mesovolume
$Q_f$	Thermal flux
$Q$ $Q_g^{\text{macro}}, Q_{\text{jump}}^{\text{macro}}$	Combustion heat Heat fluxes due to chemical reaction, and temperature jump
$b_u;$ $b_u^{-1} = \frac{2-\theta}{\theta} \sqrt{\frac{\pi}{2}}$	Slip parameter
$\theta, (0 \leq \theta \leq 1)$	Reflection coefficient
$A_T, A_{Cl}$ $b_T^{-1} = \frac{(2-a')}{a'} \sqrt{\frac{\pi}{2}} \frac{2c_p}{c_p + c_v}$	Temperature and concentration jump parameters
$a', (0 \leq a' \leq 1)$	Thermal accommodation coefficient
$A_{CO_2}; A_{O_2}$	Concentration jump of CO2 and O2 parameters
$D_T$	Thermal diffusivity coefficient
$R = 8.314 \text{ JK}^{-1} \text{ mol}^{-1}$	Gas constant
$t_0 = \frac{\exp(E/RT_0)}{k}$ $l_0 = \sqrt{\frac{\lambda_0 t_0}{c_v \rho_0}}$	Referred time and length scales for Frank-Kamenetskii variables
$t_{\text{init}}$	Ignition time